Regenerative Therapy 5 (2016) 31–39

Contents lists available at ScienceDirect

Regenerative Therapy

journal homepage: http://www.elsevier.com/locate/reth

Original article

In vivo maturation of human embryonic stem cell-derived teratoma over time

Hidenori Akutsu [a], Michiyo Nasu [a], Shojiroh Morinaga [d], Teiichi Motoyama [e], Natsumi Homma [a, f], Masakazu Machida [a], Mayu Yamazaki-Inoue [a], Kohji Okamura [b], Kazuhiko Nakabayashi [c], Shuji Takada [b], Naoko Nakamura [a], Seiichi Kanzaki [a], Kenichiro Hata [c], Akihiro Umezawa [a, *]

[a] Department of Reproductive Biology, National Research Institute for Child Health and Development, Tokyo, Japan
[b] Department of Systems BioMedicine, National Research Institute for Child Health and Development, Tokyo, Japan
[c] Department of Maternal-Fetal Biology, National Research Institute for Child Health and Development, Tokyo, Japan
[d] Department of Pathology, Kitasato Institute Hospital, Tokyo, Japan
[e] Department of Pathology, Yamagata University School of Medicine, Yamagata, Japan
[f] School of BioMedical Science, Tokyo Medical and Dental University, Tokyo, Japan

ARTICLE INFO

Article history:
Received 5 May 2016
Accepted 19 June 2016

Keywords:
Pluripotent stem cell
Next generation sequencing
Comparative genomic hybridization
Single nucleotide mutation
Nucleotide substitution rate
Morphometry

ABSTRACT

Transformation of human embryonic stem cells (hESC) is of interest to scientists who use them as a raw material for cell-processed therapeutic products. However, the WHO and ICH guidelines provide only study design advice and general principles for tumorigenicity tests. In this study, we performed in vivo tumorigenicity tests (teratoma formation) and genome-wide sequencing analysis of undifferentiated hESCs i.e. SEES-1, -2 and -3 cells. We followed up with teratoma formation histopathologically after subcutaneous injection of SEES cells into immunodeficient mice in a qualitative manner and investigated the transforming potential of the teratomas. Maturity of SEES-teratomas perceptibly increased after long-term implantation, while areas of each tissue component remained unchanged. We found neither atypical cells/structures nor cancer in the teratomas even after long-term implantation. The teratomas generated by SEES cells matured histologically over time and did not increase in size. We also analyzed genomic structures and sequences of SEES cells during cultivation by SNP bead arrays and next-generation sequencing, respectively. The nucleotide substitution rate was 3.1×10^{-9}, 4.0×10^{-9}, and 4.6×10^{-9} per each division in SEES-1, SEES-2, and SEES-3 cells, respectively. Heterozygous single-nucleotide variations were detected, but no significant homologous mutations were found. Taken together, these results imply that SEES-1, -2, and -3 cells do not exhibit in vivo transformation and in vitro genomic instability.

1. Introduction

Human embryonic stem cells (hESCs) have unique properties such as their pluripotent differentiation potential and immortality [1,2]. This capability to become a series of somatic cell types within the human body garnered significant attention and interest in the fields of regenerative medicine. The first clinical trial of hESC-based therapy started with injection of a glial cell product into patients with subacute spinal cord injury [3]. hESC-derived retinal pigmented epithelium was then developed for patients with Stargardt's macular dystrophy and dry age-related macular degeneration [4,5]. Because hESCs are used as a raw material of these cell-based products, the residual undifferentiated hESCs in the final products need to be examined for in vivo tumorigenicity [6]. Using conventional assays, malignant transformation

* Corresponding author. Department of Reproductive Biology, National Research Institute for Child Health and Development, 2-10-1 Okura, Setagaya, Tokyo, 157-8535, Japan. Tel.: +81 3 5494 7047; fax: +81 3 5494 7048.
E-mail address: umezawa@1985.jukuin.keio.ac.jp (A. Umezawa).
Peer review under responsibility of the Japanese Society for Regenerative Medicine.

http://dx.doi.org/10.1016/j.reth.2016.06.003

(generation of carcinomas, sarcomas or germ cell tumors) from hESC-teratomas has not yet been reported. When designing tumorigenicity assays, important parameters to examine include characterization of the transplanted stem cells, quantification of the number of engrafted cells, the mode and site of transplantation, monitoring of tumor formation and growth, and pathological analysis [7]. Monitoring teratomas as such is crucial, since theoretically, hESC-derived cells survive over time.

Genomic mutations may arise in hESC-derived cells during cultivation, posing an additional risk for their clinical use. Karyotypic analysis and comparative genomic hybridization (CGH) are commonly used to detect chromosomal and sub-chromosomal aberrations. Genome-wide sequencing analysis has also been applied to monitor cells in this context [8,9]. Mutation rates have been determined by various methods in human cells [10–12], and genomic sequence of hESCs has been monitored as an index for transformation and for determining nucleotide substitution rates of hESCs as compared with other cell types.

In this study, we monitored histo–pathological parameters of hESC-teratomas in vivo over time, and examined their genomic alteratiosn. We found that hESC-teratomas histologically matured over time, and that the nucleotide substitution rate in hESCs was comparable with that of somatic cells.

2. Results

Tests to detect malignant transformations include tumorigenicity test by subcutaneous implantation to immunodeficient mice. In addition to these tests, “genetic abnormality that induces persistent cell proliferation” and “genomic instability” are additional concerns. From the viewpoints of tumorigenicity of ESCs used as a starting material for manufacturing of regenerative medicine products, we herewith investigated teratoma analysis by subcutaneous implantation of SEES cells and genome-wide analysis, i.e. CGH and whole exome analysis to detect the transforming activity of the SEES cells.

2.1. Teratoma formation of SEES cells

To address whether the SEES cells (SEES-1, -2 and -3) have the competence to differentiate into specific tissues, teratomas were formed by subcutaneous implantation of SEES cells (1.0×10^7 cells/site) into immunodeficient mice (Fig. 1). Three independent clones of SEES cells induced teratomas within 6–10 weeks after implantation. Histological analysis of paraffin-embedded sections demonstrated that the three primary germ layers were generated as shown by the presence of ectodermal epidermis, glomerulus-like structure, retina, retinal pigmented epithelium, ganglion and neuroepithelium, mesodermal muscle and cartilage, and endodermal ciliated epithelium, proper gastric glands and hepatocytes in the teratomas. Thus, all SEES cell clones examined had potential for multi-lineage differentiation in vivo. We did not detect germ cell tumors, sarcomas or carcinomas in SEES-derived teratomas by histopathological analysis [13].

2.2. Morphometric analysis of teratomas

To investigate the predisposition of SEES cells to differentiate in vivo, we measured the areas of histological components such as cartilage, epidermis and intestine (Fig. 2A–E). The ratios of each component did not differ among teratomas generated by SEES-1, -2, and -3 cells (Fig. 2F–H). We also performed the same experiments using SEES cells at different PDs, i.e. short- and long-term cultivation, to investigate whether long-term cultivation affects in vivo differentiation (Fig. 3). The in vivo differentiation of SEES cells was independent of the cultivation period or passage number.

2.3. Long-term observation of teratomas generated by SEES cells

We followed up the teratomas generated by SEES cells for up to 32 weeks (Fig. 4). The maturity of hESC-teratomas clearly increased after long-term implantation, while the total area made up of each component remained unchanged. Epidermal cysts and intestines included keratinous and secretory material, respectively, and the cyst and intestinal lumen became enlarged due to accumulation of the keratinous and secretory material (Fig. 4G–J). We found neither atypical cell/structure nor cancer in the teratomas after long-term implantation.

2.4. Structural alteration analysis and exome analysis in hESCs

We performed CGH with the dye swap method on the SEES cell lines to investigate whether they had structural alterations (Fig. 5A, B). Compared to each hESC line at an early passage, we detected no chromosomal aberrations, including gain and loss, in all stocks of hESC lines (SEES-1, -2, -3). We then performed whole exome sequence analysis on the SEES cell lines to clarify the number of genetic alterations that occurred during cultivation (Fig. 5C–F). The exome analysis targeted 93.91 Mb in the genome; 21.78 Mb function as protein-coding sequences and start or stop codons (Fig. 5C). This exome study also covered a large part of the non-coding DNA sequences (non-CDS). Mapping to the reference genomic sequence hs37d5, single-nucleotide variations (SNVs) and small indels were detected at two different passages (Fig. 5D). Subsequently, the two identified genotypes at earlier and later passages were compared to find the de novo mutations occurred during the cell culture period. Because platform-specific or method-specific errors are offset in this process, reliable mutation data can be obtained. In the initial analysis of the SEES-1 line, 325 single-nucleotide and 69 indel mutations had been identified. When each genotype was examined, we noticed that a chromosome-wide mutational event causing loss of heterozygosity (LOH) occurred on the X chromosome. Hence, we also performed a structural alteration analysis by using a SNP genotyping array for all the samples. In contrast to CGH, it can also detect copy-neutral LOH with higher resolution. In SEES-1, the sole detected mutation was a deletion of one of the two X chromosomes after passage 10. Most of hetero-to-homo genotype calls on the chromosome turned out to be caused by the chromosomal deletion rather than single-nucleotide mutations. We excluded such calls and instead calculated the mutation rate of single-nucleotide substitutions. Under our cultivation conditions, one passage corresponds to approximately three population doublings (PDs). In total, 99 single bases mutated during 168 PDs in the diploid sequences of the exome targets, i.e. 3.1×10^{-9} mutations per site per PD. The numbers of mutations of SEES-2 during passages 4 and 45 were 93 single-nucleotide and 18 indel mutations (Fig. 5E). Those found in SEES-3 during passages 4 and 24 were 52 and 12 mutations, respectively. No structural mutations were detected by SNP array in the SEES-2 and SEES-3 lines. Similarly, the mutation rates of SEES-2 and SEES-3 were calculated as 4.0×10^{-9} and 4.6×10^{-9}, respectively. The regional annotation of single-nucleotide mutations shows that the number of non-synonymous bases is larger than that of synonymous bases (Fig. 5F).

We also investigated whether SEES-2 cells have mutations in cancer-related genes that are listed in the literature [14] (Supplemental Table 1). We did not find any significant homozygous nonsynonymous genetic alterations of the above-mentioned cancer-related genes in the SEES-2 cells used for teratoma formation.

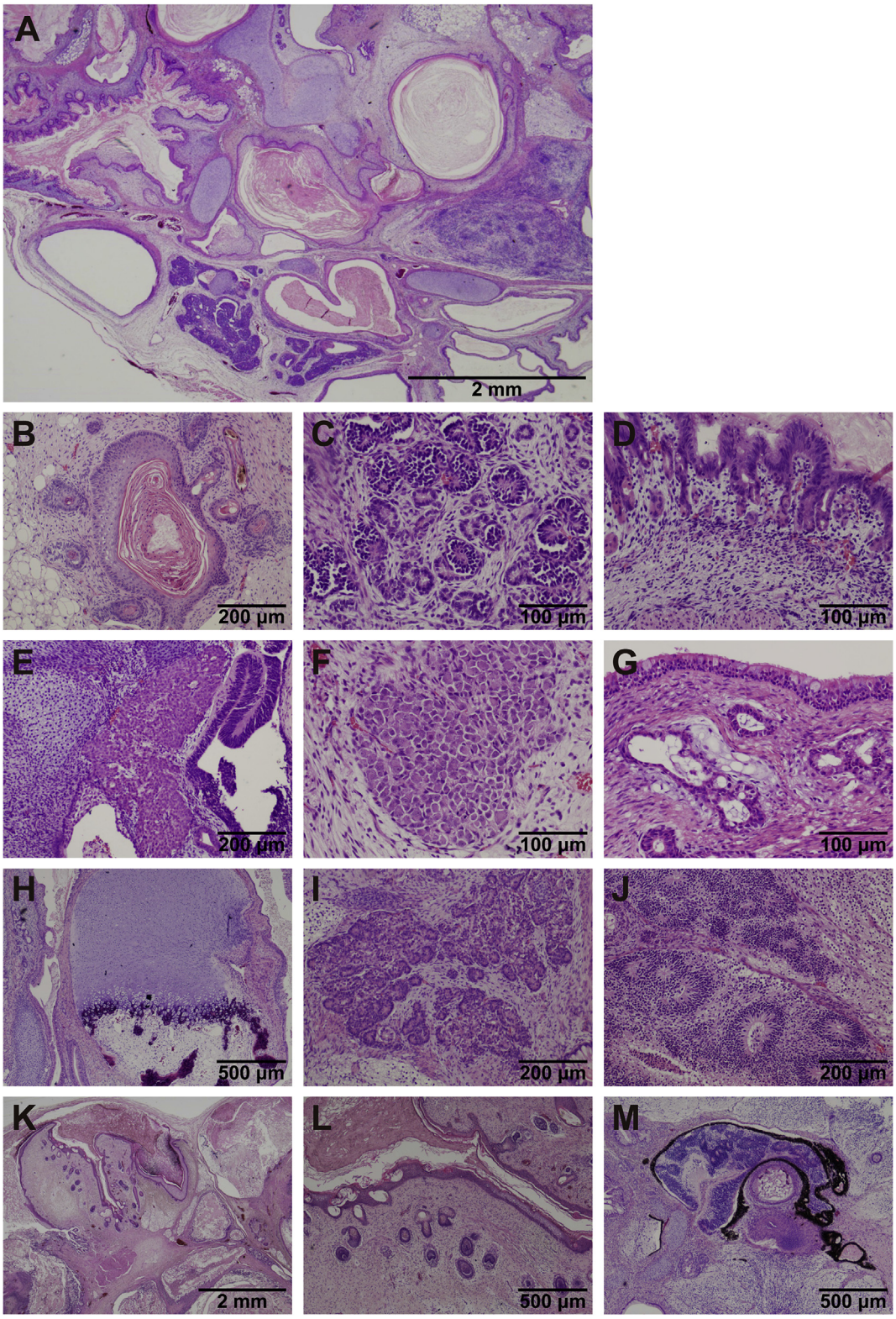

Fig. 1. In vivo pluripotency of SEES cells. A. Low power view of teratoma. B. Epidermis with keratinization. C. Glomerulus-like structure (quasi-glomerulus). D. Proper gastric glands. E. Hepatocytes. F. Ganglion. G. Tracheobronchial tissue-like structure with ciliated epithelium and glands. H. Cartilage and bone. I. Glandular structure (quasi-pancreas). J. Immature neuroepithelium. K and L. Hair follicles K: low-power view, L: high-power view. M. Retina and retinal pigmented epithelium.

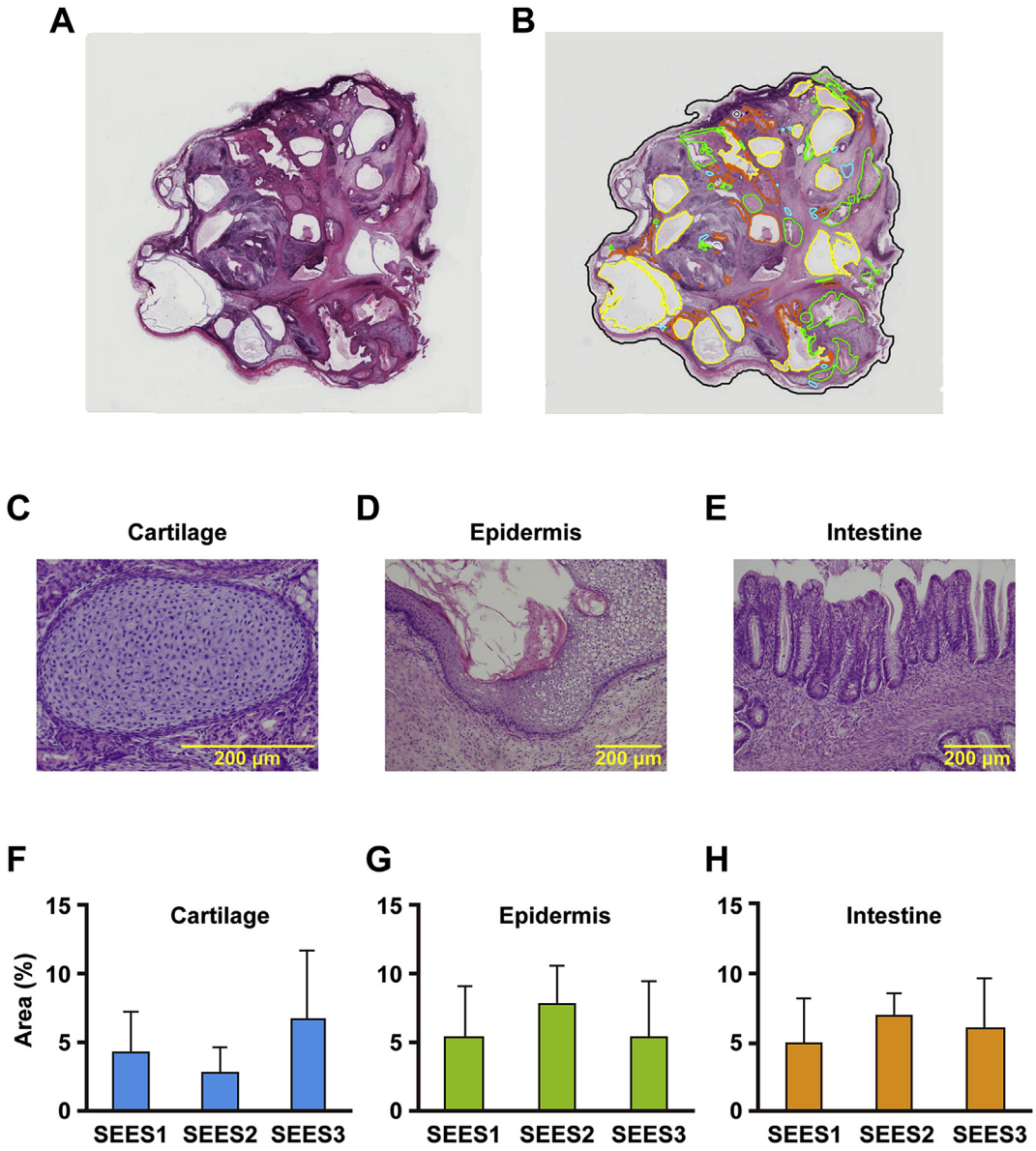

Fig. 2. Morphometric analysis of teratoma. A. Hematoxylin and eosin stain of teratoma. B. Morphometric analysis of teratoma. Total area: (area defined by black lines) minus (cystic area defined by yellow lines), cartilage: area defined by blue lines, epidermis: area defined by green lines, intestine: area defined by orange lines. C. Representative image of cartilage as defined by blue lines in panel B. D. Representative image of epidermis as defined by green lines in panel B. E. Representative image of intestine as defined by orange lines in panel B. F. Percentage of cartilage area in teratomas generated by each hES cell. Values between the indicated hES cell lines were statistically insignificant with $p < 0.01$ by Student's t-test (SEES-1 versus SEES-2, $p = 0.39$; SEES-1 versus SEES-3, $p = 0.15$; SEES-2 versus SEES-3, $p = 0.10$). G. Percentage of epidermis area in teratomas generated by each hES cell. Values between the indicated hES cell lines were statistically insignificant with $p < 0.01$ by Student's t-test (SEES-1 versus SEES-2, $p = 0.23$; SEES-1 versus SEES-3, $p = 0.76$; SEES-2 versus SEES-3, $p = 0.13$). H. Percentage of intestine area in teratomas generated by each hES cell. Values between the indicated hES cell lines were statistically insignificant with $p < 0.01$ by Student's t-test (SEES-1 versus SEES-2, $p = 0.20$; SEES-1 versus SEES-3, $p = 0.38$; SEES-2 versus SEES-3, $p = 0.56$).

3. Discussion

3.1. Do SEES teratomas mature over time?

It is not surprising that SEES teratoma included mature tissues, i.e. epidermis, retina, retinal pigmented epithelium, cartilage, ciliated epithelium, proper gastric glands and hepatocytes, as well as immature neural tissue regardless of the SEES cell lines used. The unchanged histological component ratio of ectodermal, mesodermal, and endodermal origins in the teratomas after long-term in vitro replication of SEES cells, i.e. more than 100 PDs, clearly indicates maintenance of multipotency of hESCs with immortality under the appropriate cultivation conditions. It is noteworthy that SEES teratomas often included immature glomeruli that are rarely seen in human teratoma. Lack of atypical cells/cancer cells in SEES teratoma is also not surprising because hESCs are considered intact cells that are not infected by exogenous genes such as oncogenes, unlike induced pluripotent stem cells [15–17]. Histological diagnosis of the tumors generated by SEES cells was, in all cases, immature teratoma [13,18]. Immature teratoma is typically malignant and is more often found in men, while an immature teratoma in children often behaves like a benign tumor. It is thus one of interest in this study whether SEES teratomas show maturity or immaturity during long-term implantation. SEES teratoma indeed exhibited in vivo maturation, including neural tissue. The in vivo maturation of SEES teratoma over time is preferable when SEES

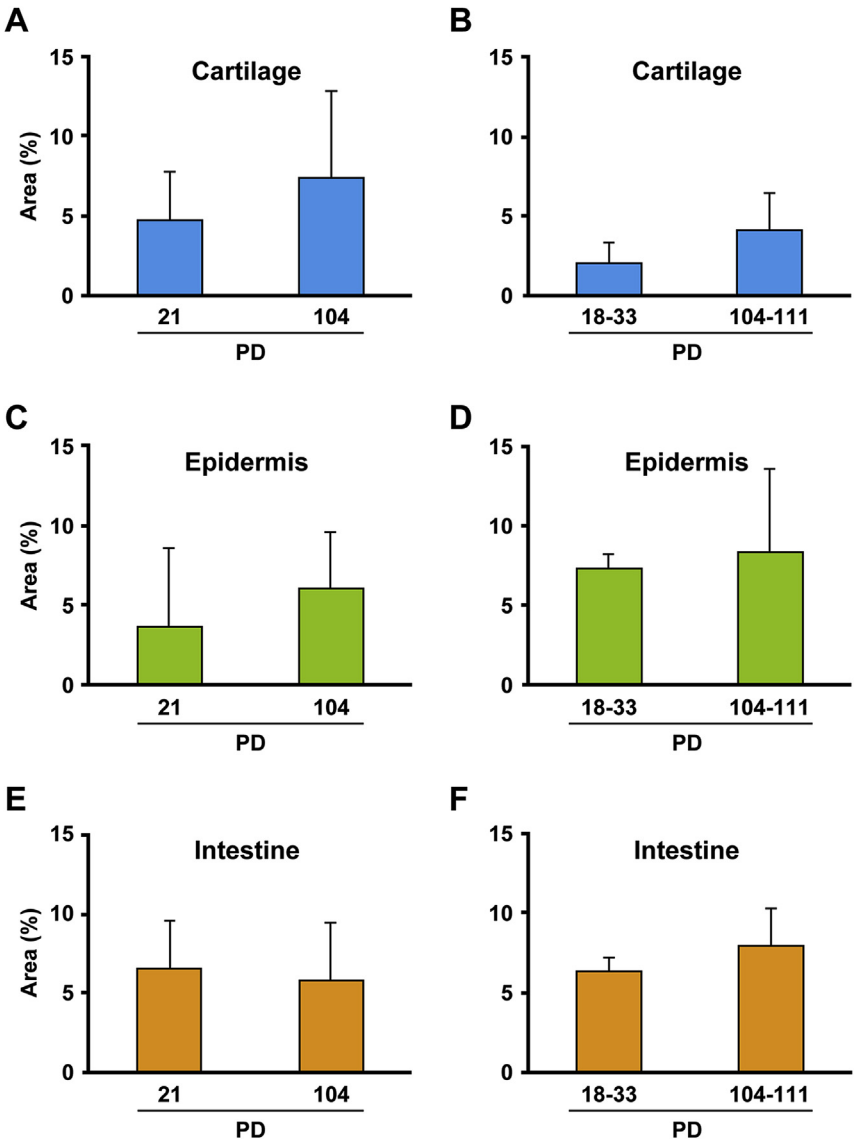

Fig. 3. Effect of long cultivation of hESCs on component area of teratoma. SEES-2 cells at population doublings (PD) 21 and PD 104, and SEES-3 cells at PD 18-33 and PD 104-111 were implanted to generate teratomas. Histological components of teratomas were morphometrically analyzed as described in Materials and Methods and in the legend for Fig. 2. A. Percentage of cartilage area in teratomas generated by SEES-2 cells. Values between PD 21 and PD 104 were statistically insignificant with $p < 0.01$ by Student's t-test ($p = 0.28$). B. Percentage of cartilage area in teratomas generated by SEES-3 cells. Values between PD 18-33 and PD 104-111 were statistically insignificant with $p < 0.01$ by Student's t-test ($p = 0.24$). C. Percentage of epidermis area in teratomas generated by SEES-2 cells. Values between PD 21 and PD 104 were statistically insignificant with $p < 0.01$ by Student's t-test ($p = 0.74$). D. Percentage of epidermis area in teratomas generated by SEES-3 cells. Values between PD 18-33 and PD 104-111 were statistically insignificant with $p < 0.01$ by Student's t-test ($p = 0.18$). E. Percentage of intestine area in teratomas generated by SEES-2 cells. Values between PD 21 and PD 104 were statistically insignificant with $p < 0.01$ by Student's t-test ($p = 0.32$). F. Percentage of intestine area in teratomas generated by SEES-3 cells. Values between PD 18-33 and PD 104-111 were statistically insignificant with $p < 0.01$ by Student's t-test ($p = 0.63$).

cells are used as a raw material of cell-based products for regenerative medicine. Residual undifferentiated ESCs during generation of cellular and tissue-based products are expected to remain benign after implantation.

3.2. Subchromosomal analysis of hESC genome

To investigate genomic alterations in cellular and tissue-based products, karyotypic analysis has been used because it is one of the most trustworthy methods. In addition to karyotypic analysis, we also utilized CGH analysis for determining the genomic stability of hESCs [19]. CGH analysis can be used for a genetically homogeneous population that has been generated by predominant proliferation or when the cultivation procedure includes subcloning of cells. Proliferating hESCs are usually passaged by choosing several single colonies, and is thus applicable to CGH analysis. From the viewpoint of genetic validation for regenerative medicine, CGH analysis may soon dominate because it is inexpensive, fast and simple.

3.3. Comparable mutation rate in hESCs

Mutation rate per nucleotide has been estimated in human cells per generation [20], in human somatic cells [11], and during the reprogramming of human somatic cells into iPSCs [21]. Different methods have been applied to determine mutation rate as sequence techniques have been dramatically developing. For this reason, it is difficult to simply compare mutation rate in cells and

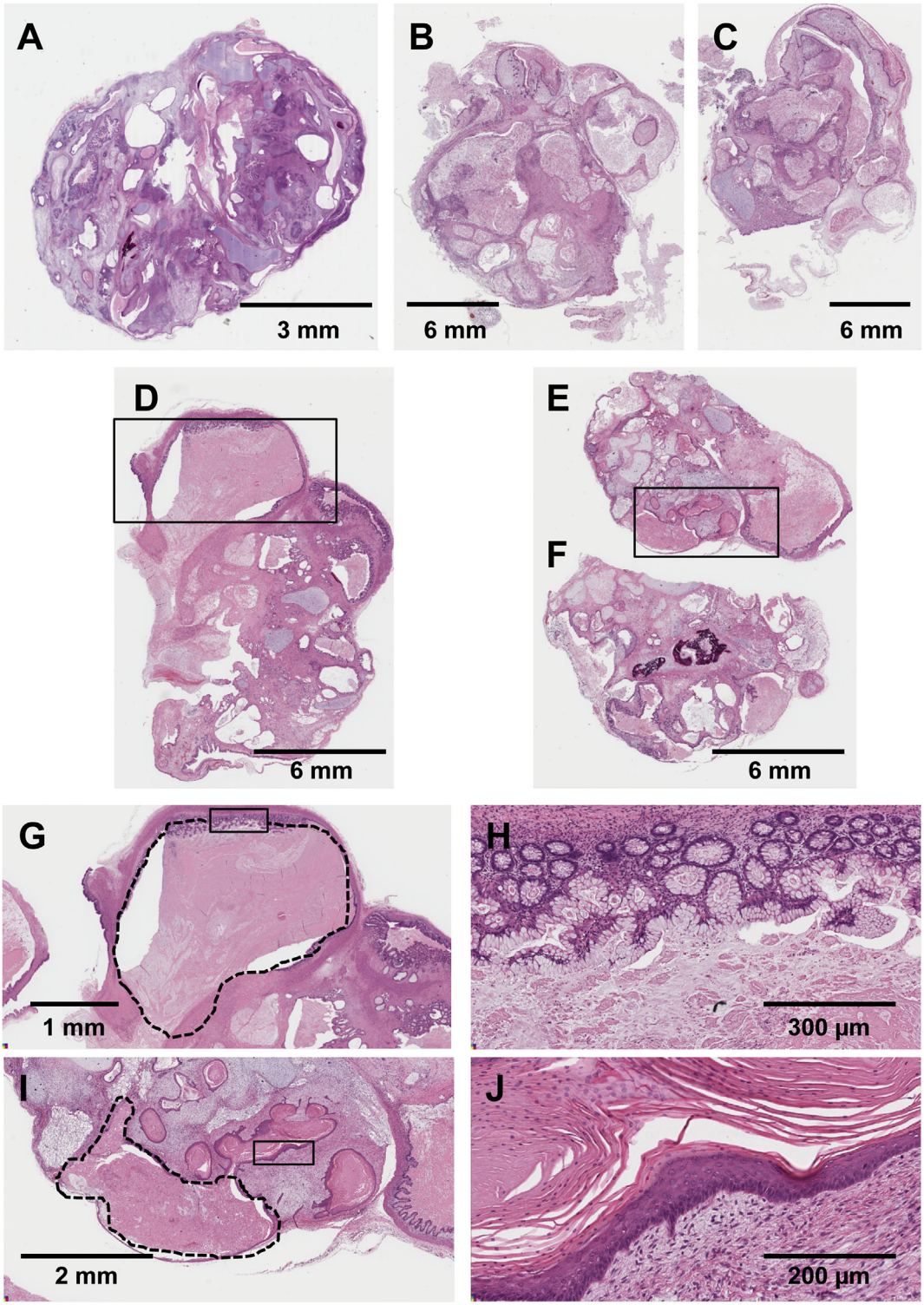

Fig. 4. In vivo maturation of SEES teratoma. A. Teratoma at 17 weeks after implantation of SEES-3 cells. B, C. Teratomas at 31 weeks after implantation of SEES-3 cells. D, E, F. Teratomas at 32 weeks after implantation of SEEDS-3 cells. G. High power view of intestinal epithelium (inlet in panel D). Dashed line: the intestinal lumen became enlarged due to accumulation of the mucus. H. High power view of intestinal epithelium (inlet in panel G). Note that intestinal epithelium were fully differentiated. I. High power view of epidermis with prominent keratinization (inlet in panel E). Dashed line: the epidermal cyst became enlarged due to accumulation of the keratinizing material. J. High power view of epidermis with distinct 4 layers, i.e. basal, spinous, granular, and horny layers (the inlet in panel I).

individuals, but it is important to estimate and validate mutation rate in hESCs as well. Whole exome analysis was used to estimate mutation rate in hESCs in this study because of its inexpensiveness and straightforwardness. The mutation rate of SEES-1 may be underestimated by the deletion of the X chromosome. Because number of passages for the SEES-3 was relatively small, the margin of error could be larger than those of SEES-1 and SEES-2. In any case, the mutation rates calculated from the three SEES lines were

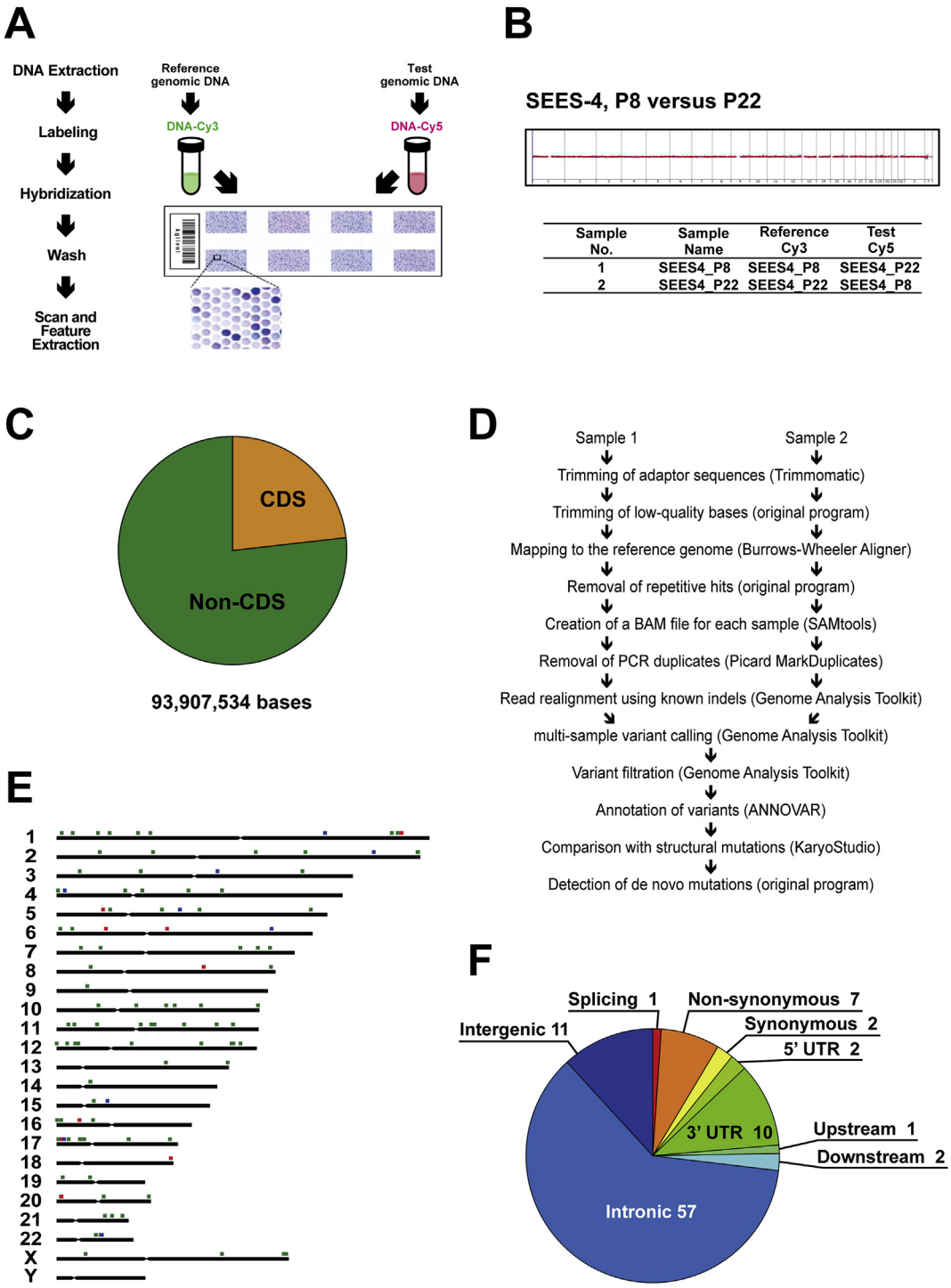

Fig. 5. Comparative genomic hybridization (CGH) in SEES cell cultivation. A. Scheme of CGH analysis. B. CGH analysis between SEES-4 cells at Passage (P) 8 and 22. C. Exome analysis of SEES cells Pie chart illustrates the ratio of protein-coding and non-coding bases. Our exome analysis targeted 93.908 Mb in the genome; 21.780 Mb out of them function as part of coding DNA sequences, start or stop codons, indicated as CDS in the figure. The present exome study covers a large part of non-coding DNA sequences (non-CDS). D. Flow chart showing each step of the exome analysis. Program names used in the present study are parenthesized. FASTQ files of sample 1 and sample 2 were separately processed and converted to BAM files. Variants, in other words, SNVs and indels, were called by comparison to the human reference genome (hs37d5). De novo mutations caused during the ESC culture were detected by subtraction of called variants in sample 2 and sample 1. Because platform-specific errors were offset, relatively accurate data were obtained. Variants found in a structural mutation, such as deletion, copy-number gain, and copy-neutral LOH, were removed for the mutation counting. E. Genome-wide distribution of the mutations identified in the SEES-2 exome analysis. Filled squares above each chromosomal bar stand for genomic positions of mutations. Green, blue, and red squares indicate single-nucleotide substitution, short insertion, and short deletion, respectively. F. Regional annotation of single-nucleotide mutations caused during the SEES-2 culture (41 passages). Note that the number of non-synonymous bases is larger than that of synonymous bases. Annotations were performed using ANNOVAR.

all approximately 4×10^{-9} mutations per site per PD, which is comparable with what is reported for human somatic mutation rates. Numbers of small-scale indel mutations detected by the present methods were much smaller than those of single-nucleotide substitution mutations. Only a few large-scale structural mutations were detected by CGH and SNP array in the present study, suggesting genetic stability of these ES cell lines.

3.4. Tumorigenicity of undifferentiated ESCs as a starting material for regenerative medicine products/cellular and tissue-based products

Undifferentiated ESCs remaining in final products after manufacturing may produce teratomas in patients and be related to increased tumorigenicity. Although it is difficult to completely eliminate a risk of transformation, in this study, we revealed the low risk of human ESCs by a qualitative follow-up study of teratomas by genomic structure and sequence analysis. Effort should be made to investigate, estimate and reduce the risk of tumorigenicity by use of currently available means to a reasonable extent [22].

4. Materials and methods

4.1. hESC culture

The ethics committee of the NCCHD specifically approved this study. The derivation and cultivation of hESC lines were performed in full compliance with “the Guidelines for Derivation and Distribution of Human Embryonic Stem Cells (Notification of the Ministry of Education, Culture, Sports, Science, and Technology in Japan (MEXT), No. 156 of August 21, 2009; Notification of MEXT, No. 86 of May 20, 2010) and “the Guidelines for Utilization of Human Embryonic Stem Cells (Notification of MEXT, No. 157 of August 21, 2009; Notification of MEXT, No. 87 of May 20, 2010)”. Human ESCs, i.e. SEES-1, -2, and -3, were used in this study. SEES lines were routinely cultured onto a feeder layer of freshly plated gamma-irradiated mouse embryonic fibroblasts, isolated from ICR embryos at 12.5 gestations and passages 2 times before irradiation (30 Gy), in the hESC culture media. The hESC media consisted of Knockout™-Dulbecco's modified Eagle's medium (KO-DMEM) (Life Technologies, CA, USA; #10829-018) supplemented with 20% Knockout™-Serum Replacement (KO-SR; #10828-028), 2 mM Glutamax-I (#35050-079), 0.1 mM non-essential amino acids (NEAA; #11140-076), 50 U/ml penicillin-50 μg/ml streptomycin (Pen-Strep) (#15070-063), 0.055 mM beta-mercaptoethanol (#21985-023) and recombinant human full-length bFGF (#PHG0261) at 10 ng/ml (all reagents from Life Technologies). Cells were expanded using STEMPRO® EZPassage™ (#23181010)/glass capillaries manually, or enzymatic passaging by Dispase II (Eidia, Ibaraki, Japan; #GD81070) [1,23].

4.2. Teratoma formation

Pluripotency in vivo was assessed by teratoma formation in immunodeficient nude mice (BALB/cAJcl-nu/nu; CLEA Japan Inc. Tokyo, Japan). A 60 mm plate of undifferentiated hESCs was washed with phosphate-buffered saline (PBS) (Life Technologies, #14190-250) and the cells were harvested with a cell scraper. The cell suspension was collected into a 15-ml conical tube and spun down at 1000 rpm for 4 min. The cell pellet was resuspended by addition of a 1:1 mixture of hESC culture medium and Matrigel (BD Biosciences, NJ, USA #356234) to a final total volume of 400 μl. Approximately $2–5 \times 10^6$ cells in 200 μl/injection site were injected in the dorsolateral area into the subcutaneous space on both sides. Tumors were excised surgically. The total number of samples for SEES-1, SEES-2, and SEES-3 were 7, 5, and 26, respectively. The animal use protocol was approved by the Institutional Animal Care and Use Committee according the National Research Institute for Child Health and Development (NRICHD, Permit Number: A2003-002). All experiments with mice were subject to the 3 R consideration (refine, reduce replace) and all efforts were made to minimize animal suffering, and to reduce the number of animals used.

4.3. Histological analysis

The tumor-containing tissues were fixed in 4% paraformaldehyde (PFA), embedded in paraffin and serially sectioned into 5 micron sections. Every other section was mounted on slides (2–10 slides for each tumor). Various parts of the tumor were stained with hematoxylin and eosin (HE), and subjected to histological analysis by certified pathologists. Large tumors were cut in half before fixation, and each of the two halves were placed in the paraffin block so that the central parts of tumor (with the larger surface area) were face up. To enable analysis of the different parts of large tumors, the sectioning was performed from the upper part of the paraffin block, containing the central parts of both halves of the tumor, towards the tumor's edges. The micoscopic images of teratomas were digitally marked by the pen tool of the Aperio ImageScope software (version 11.2.0.780). The area was automatically calculated after marking.

4.4. Array comparative genomic hybridization (aCGH)

To analyze genomic structural variants, we chose Agilent SurePrint G3 Mouse Microarray 8×60 K array technology for aCGH analysis [19]. Test and reference genomic DNAs (250 ng per sample) of human ESCs were fluorescently labeled with Cy5 (test: passage 4 of SEES-2) and Cy3 (reference: passage 24 of SEES-2) with a Genomic DNA Enzymatic Labeling Kit (Agilent Technologies). All array hybridizations were performed according to the manufacturer's methods. All regions of statistically significant copy number change were determined using Aberration Detection Method-2 (ADM2) algorithms [24]. The ADM2 algorithms identify genomic regions with copy-number differences between the test and the reference based on log2 ratios of fluorescent signals from probes in the interval.

4.5. Exome sequencing

Approximately 2.0 μg of genomic DNA from each cell sample was sonicated to give a fragment size of 200 bp on a Covaris S220 instrument. After 5–6 cycles of PCR amplification, capture and library preparation were performed with Agilent SureSelect Human All Exon V4 + UTRs + lincRNA (80 Mb), followed by washing, elution, and additional 10-cycle PCR. Enriched libraries were sequenced on an Illumina HiSeq 1000 operated in 101-bp paired-end mode. Image analyses and base calling on all lanes of data were performed using CASAVA 1.8.2 with default parameters.

4.6. Read mapping and variant analysis

Reads from each sample were first trimmed by removing adapters and low quality bases at ends using Trimmomatic 0.22 and then aligned to the hs37d5 sequence (hg19 and decoy sequences) using the Burrows-Wheeler Aligner 0.6.2. Uniquely mapped reads were selected by a custom script, converted from sam to bam using SAMtools 0.1.18, and processed by Picard 1.83 to remove PCR duplicates. Genome Analysis Toolkit (GATK) 2.4.9–3 was then used to perform local realignment and map quality score recalibration to produce calibrated bam files for each sample. Multi-sample calls for

SNVs were made by GATK. The annotated VCF files were then filtered using GATK with a stringent filter setting and custom scripts. Variant calls which failed to pass the following filters were eliminated: QUAL <400 || QD < 2.0 || MQ < 40.0 || FS > 60.0 || HaplotypeScore >13.0 || GQ ≤ 60. When genotype is 0/1, 0/2, or 1/2, only SNVs that meet the following conditions were selected: both of the allelic depths ≥ 8 && difference of the allelic depths within twofold. When genotype is 0/0, 1/1, or 2/2, only SNVs that meet the following conditions were selected: difference of the allelic depths no less than 32-fold, one allelic depth is 1 and the other is no less than 16, or one allelic depth is 0 and the other is no less than 8. Annotations of altered bases were made using ANNOVER based on GRCh37 Custom Perl scripts and C programs are available at http://github.com/glires/genomics/.

4.7. Structural mutation analysis

The structural mutation analysis by genome-wide SNP genotyping was performed using Illumina HumanCytoSNP-12 v2.1 DNA Analysis BeadChip Kit. The microarray contains approximately 300,000 SNP markers with an average call frequency of >99%. Subsequent computational and manual analyses were performed using the Illumina KaryoStudio software.

Acknowledgments

We would like to express our sincere thanks to Y. Sajima and H. Abe for providing expert technical assistance, to Dr. C. Ketcham for English editing and proofreading, and to E. Suzuki, Y. Suehiro, and K. Saito for secretarial work. This research was supported by grants from the Ministry of Education, Culture, Sports, Science, and Technology (MEXT) of Japan; by Ministry of Health, Labour and Welfare (MHLW) Sciences research grants; by a Research Grant on Health Science focusing on Drug Innovation from the Japan Health Science Foundation; by the program for the promotion of Fundamental Studies in Health Science of the Pharmaceuticals and Medical Devices Agency; by the Grant of National Center for Child Health and Development; by Research Seeds Quest Program from the Japan Science and Technology Agency (JST). We acknowledge the International High Cited Research Group (IHCRG #14-104), Deanship of Scientific Research, King Saudi University, Riyadh, Kingdom of Saudi Arabia. AU thanks King Saud University, Riyadh, Kingdom of Saudi Arabia, for the Visiting Professorship.

Appendix A. Supplementary data

Supplementary data related to this article can be found at http://dx.doi.org/10.1016/j.reth.2016.06.003.

Conflict of interest

The authors declare that they have no conflict of interest.

References

[1] Suemori H, Yasuchika K, Hasegawa K, Fujioka T, Tsuneyoshi N, Nakatsuji N. Efficient establishment of human embryonic stem cell lines and long-term maintenance with stable karyotype by enzymatic bulk passage. Biochem Biophys Res Commun 2006;345(3):926–32. http://dx.doi.org/10.1016/j.bbrc.2006.04.135. PubMed PMID: 16707099.

[2] Thomson JA, Itskovitz-Eldor J, Shapiro SS, Waknitz MA, Swiergiel JJ, Marshall VS, et al. Embryonic stem cell lines derived from human blastocysts. Science 1998;282(5391):1145–7. PubMed PMID: 9804556.

[3] Geron. Safety study of GRNOPC1 in spinal cord injury. 2010. Available from: http://clinicaltrials.gov/ct2/show/study/NCT01217008.

[4] Schwartz SD, Hubschman JP, Heilwell G, Franco-Cardenas V, Pan CK, Ostrick RM, et al. Embryonic stem cell trials for macular degeneration: a preliminary report. Lancet 2012;379(9817):713–20. http://dx.doi.org/10.1016/S0140-6736(12)60028-2. PubMed PMID: 22281388.

[5] Schwartz SD, Regillo CD, Lam BL, Eliott D, Rosenfeld PJ, Gregori NZ, et al. Human embryonic stem cell-derived retinal pigment epithelium in patients with age-related macular degeneration and Stargardt's macular dystrophy: follow-up of two open-label phase 1/2 studies. Lancet 2014. http://dx.doi.org/10.1016/S0140-6736(14)61376-3. PubMed PMID: 25458728.

[6] Recommendations for the evaluation of animal cell cultures as substrates for the manufacture of biological medicinal products and for the characterization of cell banks: Proposed replacement of TRS 878, Annex 1. World Health Organization; 2010.

[7] Sallam K, Wu JC. Embryonic stem cell biology: insights from molecular imaging. Methods Mol Biol 2010;660:185–99. http://dx.doi.org/10.1007/978-1-60761-705-1_12. PubMed PMID: 20680820.

[8] Okamura K, Toyoda M, Hata K, Nakabayashi K, Umezawa A. Whole-exome sequencing of fibroblast and its iPS cell lines derived from a patient diagnosed with xeroderma pigmentosum. Genom Data 2015;6:4–6. http://dx.doi.org/10.1016/j.gdata.2015.07.008. PubMed PMID: 26697316; PubMed Central PMCID: PMCPMC4664661.

[9] Fukawatase Y, Toyoda M, Okamura K, Nakamura K, Nakabayashi K, Takada S, et al. Ataxia telangiectasia derived iPS cells show preserved x-ray sensitivity and decreased chromosomal instability. Sci Rep 2014;4:5421. http://dx.doi.org/10.1038/srep05421. PubMed PMID: 24970375; PubMed Central PMCID: PMCPMC4073166.

[10] Roach JC, Glusman G, Smit AF, Huff CD, Hubley R, Shannon PT, et al. Analysis of genetic inheritance in a family quartet by whole-genome sequencing. Science 2010;328(5978):636–9. http://dx.doi.org/10.1126/science.1186802. PubMed PMID: 20220176; PubMed Central PMCID: PMCPMC3037280.

[11] Kuick RD, Neel JV, Strahler JR, Chu EH, Bargal R, Fox DA, et al. Similarity of spontaneous germinal and in vitro somatic cell mutation rates in humans: implications for carcinogenesis and for the role of exogenous factors in "spontaneous" germinal mutagenesis. Proc Natl Acad Sci U. S. A 1992;89(15):7036–40. PubMed PMID: 1495998; PubMed Central PMCID: PMCPMC49640.

[12] Jackson AL, Loeb LA. The mutation rate and cancer. Genetics 1998;148(4):1483–90. PubMed PMID: 9560368; PubMed Central PMCID: PMCPMC1460096.

[13] Tavassoli FA. Tumours of the ovary and peritoneum. Pathology and genetics of tumours of the breast & female genital organs. World Health Organization; 2003. p. 168–75.

[14] Walker EJ, Zhang C, Castelo-Branco P, Hawkins C, Wilson W, Zhukova N, et al. Monoallelic expression determines oncogenic progression and outcome in benign and malignant brain tumors. Cancer Res 2012;72(3):636–44. http://dx.doi.org/10.1158/0008-5472.CAN-11-2266. PubMed PMID: 22144470.

[15] Higuchi A, Ling QD, Kumar SS, Munusamy MA, Alarfaj AA, Chang Y, et al. Generation of pluripotent stem cells without the use of genetic material. Lab Invest 2015;95(1):26–42. http://dx.doi.org/10.1038/labinvest.2014.132. PubMed PMID: 25365202.

[16] De Assuncao TM, Sun Y, Jalan-Sakrikar N, Drinane MC, Huang BQ, Li Y, et al. Development and characterization of human-induced pluripotent stem cell-derived cholangiocytes. Lab Invest 2015;95(6):684–96. http://dx.doi.org/10.1038/labinvest.2015.51. PubMed PMID: 25867762; PubMed Central PMCID: PMCPMC4447567.

[17] Santostefano KE, Hamazaki T, Biel NM, Jin S, Umezawa A, Terada N. A practical guide to induced pluripotent stem cell research using patient samples. Lab Invest 2015;95(1):4–13. http://dx.doi.org/10.1038/labinvest.2014.104. PubMed PMID: 25089770.

[18] Norris HJ, Zirkin HJ, Benson WL. Immature (malignant) teratoma of the ovary: a clinical and pathologic study of 58 cases. Cancer 1976;37(5):2359–72. PubMed PMID: 1260722.

[19] Trask BJ. Fluorescence in situ hybridization: applications in cytogenetics and gene mapping. Trends Genet 1991;7(5):149–54. PubMed PMID: 2068787.

[20] Nachman MW, Crowell SL. Estimate of the mutation rate per nucleotide in humans. Genetics 2000;156(1):297–304. PubMed PMID: 10978293; PubMed Central PMCID: PMCPMC1461236.

[21] Ji J, Ng SH, Sharma V, Neculai D, Hussein S, Sam M, et al. Elevated coding mutation rate during the reprogramming of human somatic cells into induced pluripotent stem cells. Stem Cells 2012;30(3):435–40. http://dx.doi.org/10.1002/stem. 1011. PubMed PMID: 22162363.

[22] Hayakawa T, Aoi T, Umezawa A, Ozawa K, Sato Y, Sawa Y, et al. A study on ensuring the quality and safety of pharmaceuticals and medical devices derived from processing of autologous human induced pluripotent stem(-like) cells. Regen Ther 2015;2:70–80. http://dx.doi.org/10.1016/j.reth.2015.06.002.

[23] Akutsu H, Machida M, Kanzaki S, Sugawara T, Ohkura T, Nakamura N, et al. Xenogeneic-free defined conditions for derivation and expansion of human embryonic stem cells with mesenchymal stem cells. Regen Ther 2015;1:18–29.

[24] Lipson D, Aumann Y, Ben-Dor A, Linial N, Yakhini Z. Efficient calculation of interval scores for DNA copy number data analysis. J Comput Biol 2006;13(2):215–28. http://dx.doi.org/10.1089/cmb.2006.13.215. PubMed PMID: 16597236.